Reaction Front Evolution during Electrochemical Lithiation of Crystalline Silicon Nanopillars

Seok Woo Lee,[a] Lucas A. Berla,[a] Matthew T. McDowell,[a] William D. Nix,[a] and Yi Cui*[a, b]

Abstract: The high theoretical specific capacity of Si as an anode material is attractive in lithium-ion batteries, although the issues caused by large volume changes during cycling have been a major challenge. Efforts have been devoted to understanding how diffusion-induced stresses cause fracture, but recent observations of anisotropic volume expansion in single-crystalline Si nanostructures require new theoretical considerations of expansion behavior during lithiation. Further experimental investigation is also necessary to better understand the anisotropy of the lithiation process. Here, we present a method to reveal the crystalline core of partially lithiated Si nanopillars with three different crystallographic orientations by using methanol to dissolve the Li atoms from the amorphous Li-Si alloy. The exposed crystalline cores have flat {110} surfaces at the pillar sidewalls; these surfaces represent the position of the reaction front between the crystalline core and the amorphous Li-Si alloy. It was also found that an amorphous Si structure remained on the flat surfaces of the crystalline core after dissolution of the Li, which was presumed to be caused by the accumulation of Si atoms left over from the removal of Li from the Li-Si alloy.

Keywords: anisotropic expansion · electrochemistry · lithium-ion batteries · nanostructures · reaction mechanisms

1. Introduction

Silicon is one of the most promising anode materials for use in rechargeable lithium-ion batteries due to its high theoretical specific capacity of $4200\,mAh\,g^{-1}$ and low cost.[1] However, this high lithium storage capacity results in enormous volume expansion and contraction during electrochemical lithiation and delithiation, which can induce mechanical fracture and severe capacity fading.[2] Recently, studies have utilized Si nanostructures, such as nanowires, nanotubes, and nanoparticles, to improve cycling performance; these nanostructures have greater fracture resistance than larger particles because lower stresses are created in the nanostructures during the volume changes.[3] Despite an abundance of research on electrochemical insertion/extraction of Li into/from Si nanostructures, fracture of these nanostructures is not yet completely understood. Further research on the Li-Si alloying process is necessary to understand how nanostructure dimensions, morphology, and crystalline orientation affect the fracture of these structures during lithiation and delithiation. In order to understand the fracture of Si electrodes during electrochemical Li insertion, various theoretical models have been proposed. Most models describe fracture as resulting from diffusion-induced stresses and assume that the process of lithiation is isotropic.[4] These theories do not take into account the experimentally observed anisotropic volume expansion behavior along $<110>$ directions or the two-phase reaction boundary separating crystalline Si from amorphous Li-Si during lithiation.[5] Furthermore, recent studies have shown that single-crystalline Si nanostructures have a tendency to fracture between neighboring {110} surfaces during lithiation because of intensified tensile hoop stresses induced by anisotropic volume expansion.[6] To approach these issues, Zhao et al. have developed a model of concurrent reaction and plasticity considering a sharp phase boundary between the crystalline Si and the lithiated Si.[7] They explained how tensile hoop stresses develop at the particle surface and also estimated the shape of the crystalline core and the extent of anisotropic volume expansion during partial lithiation. A different in situ transmission electron microscopy study of the lithiation of crystalline Si nanoparticles showed that the crystalline core becomes noticeably faceted as it shrinks due to anisotropic volume expansion.[6a] To build on this and to develop a better understanding of the lithiation process, it would

[a] S. W. Lee, L. A. Berla, M. T. McDowell, W. D. Nix, Y. Cui
Department of Materials Science and Engineering
Stanford University, Stanford, CA 94305 (USA)
e-mail: yicui@stanford.edu

[b] Y. Cui
Stanford Institute for Materials and Energy Sciences
SLAC National Accelerator Laboratory, 2575 Sand Hill Road,
Menlo Park, CA 94025 (USA)

be informative to systematically monitor the crystalline core shapes in well-defined single-crystalline nanostructures as lithiation progresses. Here, we present a method for revealing the crystalline core of partially lithiated Si nanopillars of three different crystal orientations. Using methanol, we are able to remove the amorphous Li-Si shell on the outside of partially lithiated Si nanopillars, thereby revealing the shapes of the crystalline cores. We note that water has too high reactivity with lithiated silicon, which would damage the pillars. Methanol is less reactive and preserves the crystalline core.

2. Results and Discussion

Following the methods employed in previous research, the Si nanopillars used in this study were prepared by dry etching single-crystalline Si wafers of various crystal orientations ($<100>$, $<110>$, and $<111>$).[5b,8] Drop-cast silica spheres were used as an etch mask to create pillars with circular cross sections. The pillar diameters varied from 300 to 500 nm and were determined by the initial diameter of the silica spheres, and their height was around 2–3 μm. After pillar fabrication, the Si wafer on which the pillars were etched was cut into pieces with areas of ~25 mm², and these pieces were electrochemically lithiated by inserting them into half-cells with Li foil as the counter/reference electrode. Next, the potential of the silicon electrode was swept to 10 mV vs. Li/Li$^+$ at a sweep rate of 0.1 mV/s and was then held for two or three hours to cause partial lithiation, at which point a crystalline core of the pillar remains while the shell is lithiated. After electrochemical lithiation of the pillars, the half-cells were opened and the samples were washed in acetonitrile in an argon-filled glove box. In order to examine the crystalline core of partially lithiated pillars, some samples were immersed in methanol in an argon-filled glove box for as long as it took for bubble generation to terminate (30–45 s). The bubbles are hydrogen, produced by the mild reaction of lithium with methanol.[9] The remaining crystalline Si nanopillar cores were observed in a scanning electron microscope (SEM) and transmission electron microscope (TEM). Partially lithiated pillar samples that were not etched in methanol were also examined with an SEM. As Li-containing silicon alloys react rapidly in air, these samples were sealed in glass vials inside an argon-filled glove box before being transported to the SEM.

Figure 1 consists of SEM images of initially pure crystalline Si nanopillars with a $<110>$ axial orientation. Figures 1a–c show top-down SEM images of a pristine pillar, a partially lithiated pillar (120 mV for 10 hr), and a partially lithiated pillar that has been methanol etched, respectively. Although the pillars seen in Figures 1a–c are not the same pillar, each is representative of all pillars prepared using a given approach. After partial lithiation,
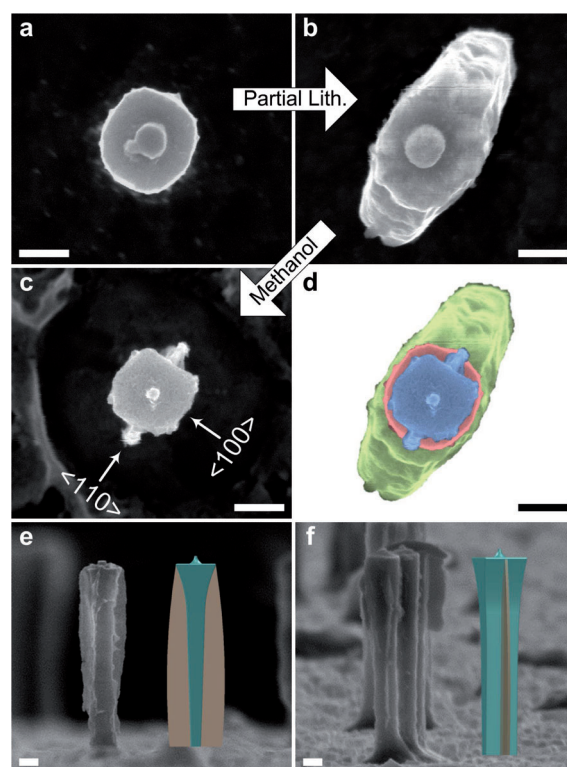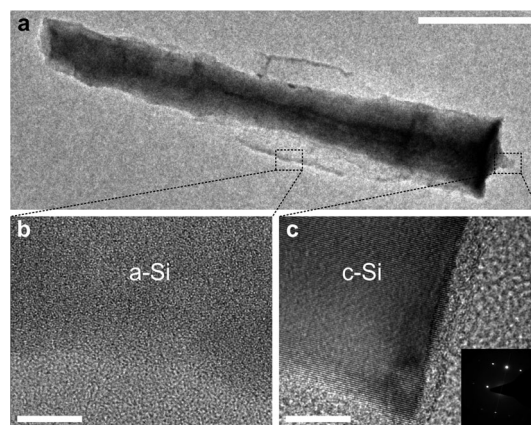

Figure 1. Partial lithiation and methanol etching of a $<110>$ Si nanopillar. Top-down SEM images of a $<110>$ Si nanopillar a) before lithiation, b) after partial lithiation, and c) after etching of the amorphous Li-Si alloy with methanol. For partial lithiation, a voltage of 120 mV vs. Li/Li$^+$ was applied for 10 hr. d) Composite false-color image merging panels a–c for dimensional comparison. e) SEM image along the $<100>$ direction, as indicated in panel c and its schematic. f) SEM image along the $<110>$ direction, as indicated in panel c and its schematic. All scale bars are 200 nm.

the initially circular pillar (Figure 1a) becomes an ellipse due to preferential expansion along the two $<110>$ directions at the pillar sidewalls, as shown in Figure 1b.[5b] After methanol etching of the amorphous Li-Si alloy, the width of the pillars is clearly reduced and a rectangular crystalline core with fin structures on the {110} sidewalls is revealed, as shown in Figure 1c. Figure 1d is a composite image in which Figures 1a–c have been merged and colored for comparison of the shapes and dimensions in each image. After partial lithiation (green), the expanded pillar has a greater width than the pristine pillar (red). After methanol etching of the amorphous Li-Si alloy surrounding the crystalline core, the width of the core (blue) is narrower than the pristine pillar, but the fin structures extend to the initial boundary of the pristine pillar. Side views of an etched $<110>$ axially oriented pillar viewed along the $<100>$ and $<110>$ directions, as indicated in Figure 1c, are shown in Figures 1e and 1f, respectively. In Figure 1e, the crystalline core is noticeably thinner due to its preferential consumption along $<110>$ directions during lithiation, and the fins are attached to the {110}

sidewalls of the crystalline core. Figure 1f shows a similar pillar viewed along a <110> direction, and it is clear that the crystalline core is thicker than in Figure 1e. A TEM micrograph providing a tilted view of an etched <110> Si pillar supports the shape of the <110> pillar established in Figures 1e and 1f (see Figure S3 in Supplementary Information).

Further characterization of these etched pillars with the TEM allows for a determination of the structure and composition. Figure 2a shows a TEM image of a pillar viewed along a <100> direction after partial lithiation and etching. The core of the pillar shows diffraction and thickness contrast, while the fins at each edge do not generate significant contrast. Figures 2b and 2c are high-resolution images of the fin and the tip of the core, respectively. The image of the fin does not contain lattice fringes, indicating that it is amorphous, and energy-dispersive X-ray spectroscopy (EDX) indicates that the dominant atomic species in the amorphous fin is Si (see Figure S4 in the Supplementary Information). The image and selected-area electron diffraction (SAED) pattern of the core of the pillar in Figure 2c show that the core is single-crystalline Si (the same as the pristine pillar). The amorphous Si fins observed on the etched pillars are probably created by the accumulation of Si atoms as the Li atoms are removed during the etching process (see Figure S5 in the Supplementary Information for further study of the mechanism).

The SEM and TEM data from <110> Si nanopillars after partial lithiation and etching of the amorphous Li-Si

Figure 2. TEM study of a <110> Si nanopillar after partial lithiation and methanol etching. a) TEM image of the remaining crystalline core and fin structure of a <110> Si nanopillar. The scale bar is 500 nm. b) High-resolution TEM (HRTEM) image of the fin structure attached to the sidewall of the core, the location of which is indicated by the dashed rectangle in panel a. The scale bar is 10 nm. c) HRTEM image of the tip of the core of the pillar. The scale bar is 10 nm. The inset image is an SAED pattern showing that the core is single-crystalline Si with an axial orientation of <110>.

alloy reveal that the cross-sectional shape of the remaining crystalline core is a rectangle with the shorter dimension along the <110> direction. To determine how anisotropic consumption affects the shape of the crystalline core of pillars with other axial orientations during lithia-
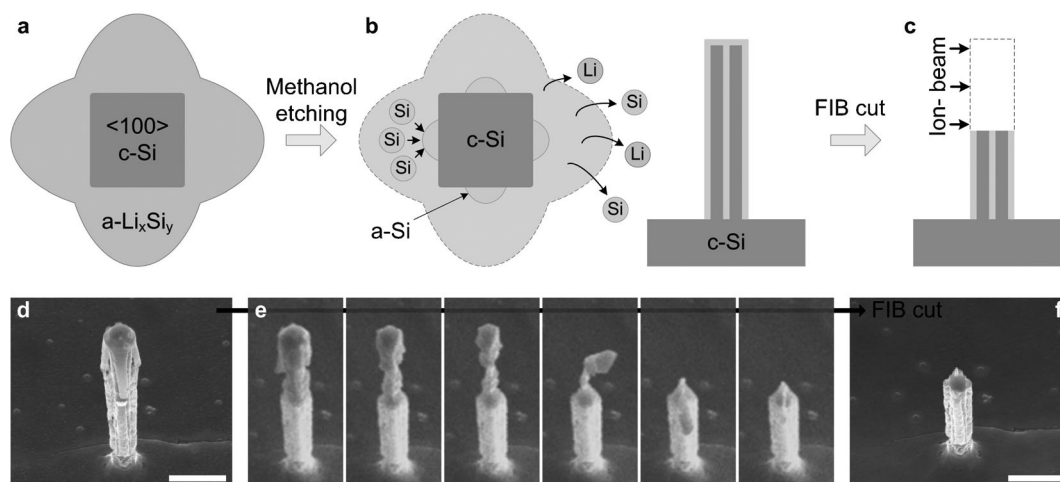

Figure 3. Using the FIB to cut the upper half of a partially lithiated <100> Si nanopillar that has been etched in methanol. The technique is utilized to better observe the cross section of the crystalline core. a–c) Schematic view of the FIB cutting technique applied to the crystalline core of a <100> pillar that remains after methanol etching. a) Upon partial lithiation, a <100> Si pillar expands to a cross-shaped structure, with a square being the anticipated shape of the crystalline core since the <100> crystalline Si pillar sidewall has four {110} surfaces. b) Li atoms in the amorphous Li-Si phase are etched away with methanol. During this etching process, Si atoms accumulate at the {110} sidewall surfaces, forming amorphous fin-like structures along these surfaces. c) The sample is loaded in the FIB so that the pillar axis is normal to the ion beam axis, and the ion beam is used to cut off the top of the pillar, which stands at the edge of the underlying substrate. d) Tilted SEM image showing a methanol-etched <100> pillar prior to FIB cutting. e) SEM images taken during exposure of the pillar to the ion beam. As a result of incomplete etching of the upper part of the pillar, a small needle falls onto and remains on the top surface of the pillar subsequent to beam exposure. f) SEM image of the pillar after FIB cutting. All scale bars are 1 μm.

tion, methanol etching of partially lithiated <100> and <111> axially oriented pillars was performed and the pillars were observed with SEM (see Figure S6 in the Supplementary Information for the results). However, the shape of the Si core is difficult to determine from these images. To unambiguously determine the shape of the crystalline core after partial lithiation, a focused ion beam (FIB) was used to cut etched pillars in half so that the cross section was visible. It was not necessary to cut the <111> pillars with FIB since the cross-sectional shape was obvious in top-down images.

For FIB cutting, pillars of three different axial orientations (<100>, <110>, and <111>) were partially lithiated at 10 mV for one or two hours. The initial diameter of the pristine crystalline Si pillars is around 500 nm. The schematic presented in Figure 3 outlines the process by which a methanol-etched <100> Si pillar is milled with FIB for top-down SEM observation of the shape of the core. After partial lithiation, the <100> pillar expands to a cross shape (Figure 3a), and the shape of the unlithiated core is shown in gray.[5b] Etching the amorphous Li-Si phase with methanol reveals the crystalline core, and amorphous Si accumulates on the four {110} sidewall faces of the core (Figure 3b). Next, as illustrated in Figure 3c, the etched pillar is mounted on an SEM holder such that the gallium ion beam is normal to the pillar axis (parallel to the plane of the underlying silicon substrate). The SEM image in Figure 3d is a picture (52° tilt) of a <100> pillar after methanol etching. Figure 3e shows several SEM images captured over the course of the FIB milling process. The top half of the pillar is visibly milled away as ion beam exposure is extended. After completion of FIB milling, the core appears to have a clean cross section suitable for top-down-view imaging.

Figure 4 shows top-down SEM images of pillars of various axial orientations after partial lithiation (Figures 4a–c) and also after etching with methanol and cutting with the FIB (Figures 4d–f). The images after FIB milling show the shape of the crystalline core. As described in a previous study,[5b] the <100>, <110> and <111> axially oriented pillars expand, respectively, into a cross shape, an ellipse, and a circle due to anisotropic expansion along <110> lateral directions. As shown in Figure 4d, methanol etching and FIB milling reveals that the <100> pillar has a square crystalline core. Amorphous Si is accumulated on the four flattened {110} surfaces of the core. The needle-like structure at the upper edge of the pillar is a fragment of amorphous Si left over from FIB milling. The crystalline core of the <110> pillar has a rectangular shape with the shorter dimension along the <110> direction (Figure 4e). The <111> pillar has a hexagonal core with flat faces orthogonal to lateral <110> directions, as shown in Figure 4f. From the shape of the crystalline core of the etched pillars, it can be concluded that {110} surfaces of crystalline Si are the favored reaction site for lithiation and volume expansion, much like
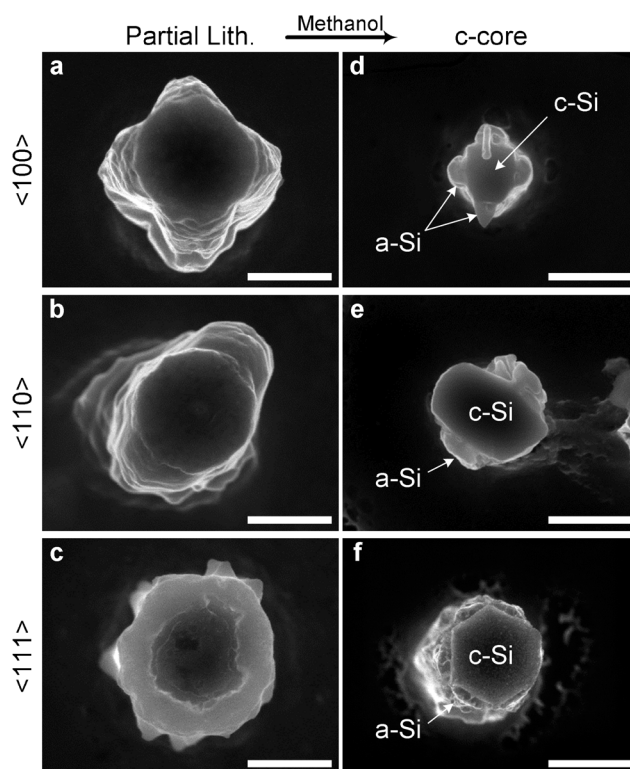
Figure 4. Si nanopillars with three different axial orientations (< 100>, <110>, and <111>) after partial lithiation and etching/FIB cutting to view the cross section. a–c) Top-down SEM images of partially lithiated Si pillars held at 10 mV vs. Li/Li$^+$ for 1–2 hr. <100>, <110>, and <111> pillars expand into a cross, an ellipse, and a circle, respectively, as shown in a previous study.[5b] d) Top-down SEM image of the cross section of a <100> pillar after FIB removal of the top half of the pillar. The four flattened edges of the crystalline core are {110} surfaces on which the residual amorphous Si fin is attached. e) Top-down SEM image of the cross section of a <110> pillar after FIB cutting. The two flattened edges of the crystalline core are the lateral {110} surfaces. f) Top-down SEM image of the cross section of a <111> pillar without FIB cutting. The six flattened edges of the crystalline core are the lateral {110} surfaces. All scale bars are 500 nm.

chemical wet etching.[10] The crystalline structure is consumed and the amorphous Li-Si alloy grows at these surfaces through the migration of a reaction front. This causes anisotropic volume expansion of the amorphous Li-Si alloy and shrinkage of the crystalline Si core along the <110> directions. The anisotropy of Si during electrochemical lithiation is probably caused by the different electrochemical potentials of the lithiation of each crystallographic Si plane, as shown using density functional theory (DFT).[11] In addition to anisotropic volume expansion, the fracture locations in crystalline silicon nanostructures are related to the anisotropy and the shape of the crystalline core. As shown in our previous study, fracture occurs at the surface between lateral {110} planes upon lithiation of the pillars.[6b] This suggests that tensile hoop stress is intensified at these locations, and the pref-

erential lithiation and volume expansion during lithiation at the flat {110} crystal facets is presumed to cause these stress concentrations.

3. Conclusions

In summary, we have investigated the process by which single-crystalline Si nanopillars are consumed during electrochemical lithiation. Methanol is used to etch the amorphous Li-Si alloy and reveal the crystalline core of the partially lithiated pillars more than showing morphology changes as reported in our previous studies.[5b,6b] It is found that the crystalline cores have particular shapes defined by flat {110} lateral surfaces for each pillar orientation. The cross sections of the <100>, <110>, and <111> pillars have square, rectangular, and hexagonal shapes, respectively, and the flat surfaces of the core are orthogonal to the <110> lateral directions in each pillar. The observed crystal shapes are consistent with anisotropic expansion of the pillars: preferential consumption of the crystalline Si at {110} lateral planes results in the reaction front proceeding further along these directions, and it flattens these planes in the process. These observations provide a better understanding of the anisotropic lithiation behavior and fracture of single crystal Si, and this knowledge can be used in the estimation of the stresses that develop in crystalline Si anodes during lithiation.

4. Experimental Section

Silica Nanoparticle Synthesis

Silica nanoparticles were produced by a modified Stöber synthesis.[12] Briefly, 1.3 mL tetraethyl orthosilicate (TEOS) was mixed with 10 mL ethanol, and then a NH_4OH/ethanol solution was added to precipitate silica. After eight hours of reaction, the spheres were centrifuged and cleaned with ethanol and methanol. Silica nanospheres of 600 nm diameter were produced.

Silicon Nanopillar Fabrication

<100>, <110>, and <111> silicon wafers (p-type, 10–20 Ω cm, 500–550 μm thick) were first cleaned with O_2 plasma for 5 min and then the colloid of silica nanospheres was dispersed on the wafer and allowed to dry. These Si wafers were then etched using the Bosch process with a Deep Reactive Ion Etcher (Surface Technology Systems Co.). SF_6 (50 sccm) and C_4H_8 (80 sccm) were used for etching and passivation with active times of 3 s and 6 s, respectively. The total etching time was 7–9 min at 350 W of RF power. After dry etching, wet etching with concentrated HF for several seconds dissolved the remaining silica nanospheres on top of the pillars.

Electrochemistry and Structural Characterization

Half-cells were made with pieces of the wafers on which Si nanopillars had been etched as the working electrode. Li foil was used as the counter/reference electrode. Polymer separators (Nagase) were placed between the two electrodes, and the sandwich structure was sealed in a pouch with external electrical leads. The electrolyte was 1 M $LiPF_6$ in ethylene carbonate/diethyl carbonate (EC/DEC, 1:1; Merck). For lithiation/delithiation, linear-sweep voltammetry was used on either a Bio-logic VMP3 battery tester or an Arbin BT2000. For partial lithiation, the voltage was swept at varying rates from the open circuit voltage to 10 mV vs. Li/Li^+, where it was held for 1–2 hr; alternatively, 120 mV vs. Li/Li^+ was applied for 10 hr. After electrochemical treatment, the nanopillar sample was removed in an Ar-filled glove box and washed with acetonitrile to eliminate residual electrolyte and SEI. The samples were then transferred to the SEM (FEI XL30 Sirion SEM) or TEM (FEI Tecnai G2 F20 X-TWIN TEM) for imaging. To minimize exposure to the air, the sample was sealed in a glass vial while still in the glove box and was then carried to the SEM or TEM.

Focused Ion Beam Cutting of the Pillars

An xP 3.35 DualBeam System (FEI Company), which is a dual FIB/SEM apparatus, was used to mill off the tops of the pillars, exposing the pillar cross sections halfway up the pillar height. Samples were mounted such that the gallium ion beam was normal to the pillar axis (parallel to the plane of the underlying silicon substrate). First, a pillar near the cleaved edge of the Si substrate was located at an ion current of 10 pA (30 kV voltage), and exposure time was minimal so as to prevent noticeable etching of the pillar at this low ion current. Then, the pillar of interest was milled at a higher ion current of 30 pA (30 kV voltage) until the upper half of the pillar was completely removed.

Author Contributions

S.W.L., L.A.B., and M.T.M. carried out the experiments. All authors analyzed the data and wrote the paper.

Acknowledgements

References

[1] a) B. A. Boukamp, G. C. Lesh, R. A. Huggins, *J. Electrochem. Soc.* **1981**, *128*, 725–729; b) M. Armand, J. M. Tarascon, *Nature* 2008, 451, 652–657; c) M. S. Whittingham, *MRS Bull.* **2008**, *33*, 411–419.

[2] a) L. Y. Beaulieu, K. W. Eberman, R. L. Turner, L. J. Krause, J. R. Dahn, *Electrochem. Solid-State Lett.* **2001**, *4*, A137-A140; b) U. Kasavajjula, C. Wang, A. J. Appleby, *J. Power Sources* **2007**, *163*, 1003–1039.

[3] a) N. Liu, H. Wu, M. T. McDowell, Y. Yao, C. Wang, Y. Cui, *Nano Lett.* **2012**, *12*, 3315–3321; b) C. K. Chan, H. Peng, G. Liu, K. McIlwrath, X. F. Zhang, R. A. Huggins, Y. Cui, *Nat. Nanotechnol.* **2008**, *3*, 31–35; c) A. Magasinski, P. Dixon, B. Hertzberg, A. Kvit, J. Ayala, G. Yushin, *Nat. Mater.* **2010**, *9*, 353–358; d) H. Kim, M. Seo, M. H. Park, J. Cho, *Angew. Chem., Int. Ed.* **2010**, *49*, 2146–2149; e) T. Song, J. L. Xia, J. H. Lee, D. H. Lee, M. S. Kwon, J. M. Choi, J. Wu, S. K. Doo, H. Chang, W. Il Park, D. S. Zang, H. Kim, Y. G. Huang, K. C. Hwang, J. A. Rogers, U. Paik, *Nano Lett.* **2010**, *10*, 1710–1716; f) Y. Yao, M. T. McDowell, I. Ryu, H. Wu, N. A. Liu, L. B. Hu, W. D. Nix, Y. Cui, *Nano Lett.* **2011**, *11*, 2949–2954; g) I. Kovalenko, B. Zdyrko, A. Magasinski, B. Hertzberg, Z. Milicev, R. Burtovyy, I. Luzinov, G. Yushin, *Science* **2011**, *334*, 75–79; h) T. H. Hwang, Y. M. Lee, B. S. Kong, J. S. Seo, J. W. Choi, *Nano Lett.* **2012**, *12*, 802–807; i) H. Wu, G. Chan, J. W. Choi, I. Ryu, Y. Yao, M. T. McDowell, S. W. Lee, A. Jackson, Y. Yang, L. Hu, Y. Cui, *Nat. Nanotechnol.* **2012**, *7*, 310–315; j) T. H. Hwang, Y. M. Lee, B. S. Kong, J. S. Seo, J. W. Choi, *Nano Lett.* **2012**, *12*, 802–807; k) H. Wu, G. Zheng, N. Liu, T. J. Carney, Y. Yang, Y. Cui, *Nano Lett.* **2012**, *12*, 904–909.

[4] a) T. K. Bhandakkar, H. Gao, *Int. J. Solids Struct.* **2011**, *48*, 2304–2309; b) I. Ryu, J. W. Choi, Y. Cui, W. D. Nix, *J. Mech. Phys. Solids* **2011**, *59*, 1717–1730; c) K. Zhao, M. Pharr, J. J. Vlassak, Z. Suo, *J. Appl. Phys.* **2010**, *108*, 073517; d) Y.-T. Cheng, M. W. Verbrugge, *J. Electrochem. Soc.* **2010**, *157*, A508–A516.

[5] a) J. L. Goldman, B. R. Long, A. A. Gewirth, R. G. Nuzzo, *Adv. Funct. Mater.* **2011**, *21*, 2412–2422; b) S. W. Lee, M. T. McDowell, J. W. Choi, Y. Cui, *Nano Lett.* **2011**, *11*, 3034–3039; c) X. H. Liu, H. Zheng, L. Zhong, S. Huang, K. Karki, L. Q. Zhang, Y. Liu, A. Kushima, W. T. Liang, J. W. Wang, J. H. Cho, E. Epstein, S. A. Dayeh, S. T. Picraux, T. Zhu, J. Li, J. P. Sullivan, J. Cumings, C. Wang, S. X. Mao, Z. Z. Ye, S. Zhang, J. Y. Huang, *Nano Lett.* **2011**, *11*, 3312–3318; d) J. Li, J. R. Dahn, *J. Electrochem. Soc.* **2007**, *154*, A156-A161; e) M. T. McDowell, S. W. Lee, I. Ryu, H. Wu, W. D. Nix, J. W. Choi, Y. Cui, *Nano Lett.* **2011**, *11*, 4018–4025.

[6] a) X. H. Liu, J. Y. Huang, *Energy Environ. Sci.* **2011**, *4*, 3844–3860; b) S. W. Lee, M. T. McDowell, L. A. Berla, W. D. Nix, Y. Cui, *Proc. Natl. Acad. Sci. U.S.A.* **2012**, *109*, 4080–4085; c) M. T. McDowell, I. Ryu, S. W. Lee, C. Wang, W. D. Nix, Y. Cui, *Adv. Mater.* **2012**, *24*, 6034–6041.

[7] K. Zhao, M. Pharr, Q. Wan, W. L. Wang, E. Kaxiras, J. J. Vlassak, Z. Suo, *J. Electrochem. Soc.* **2012**, *159*, A238–A243.

[8] C. M. Hsu, S. T. Connor, M. X. Tang, Y. Cui, *Appl. Phys. Lett.* **2008**, *93*, 133109.

[9] R. N. Castellano, P. H. Schmidt, *J. Electrochem. Soc.* **1971**, *118*, 653–654.

[10] K. E. Bean, *IEEE Trans. Electron Devices* **1978**, *25*, 1185–1193.

[11] M. K. Y. Chan, B. R. Long, A. A. Gewirth, J. P. Greeley, *J. Phys. Chem. Lett.* **2011**, *2*, 3092–3095.

[12] G. H. Bogush, M. A. Tracy, C. F. Zukoski, *J. Non-Cryst. Solids* **1988**, *104*, 95–106.